Mameka, N.; Markmann, J.; Jin, H.-J.; Weissmueller, J.:

**Electrical stiffness modulation—confirming the impact of surface excess elasticity on the mechanics of nanomaterials**

In: Acta Materialia (2014) Elsevier

DOI: 10.1016/j.actamat.2014.04.067

# Electrical stiffness modulation – confirming the impact of surface excess elasticity on the mechanics of nanomaterials

Nadiia Mameka[a,*], Jürgen Markmann[a,b], Hai-Jun Jin[c], Jörg Weissmüller[a,b]

[a] *Helmholtz-Zentrum Geesthacht, Institut für Werkstoffforschung, Werkstoffmechanik, 21502 Geesthacht, Germany*
[b] *Technische Universität Hamburg-Harburg, Institut für Werkstoffphysik und -technologie, 21073 Hamburg, Germany*
[c] *Shenyang National Laboratory for Materials Science, Institute of Metal Research, Chinese Academy of Sciences, 110016 Shenyang, People's Republic of China*

**Abstract**

Local variations of the stiffness at surfaces may affect the elastic response of nanostructures, yet experiments disagree on magnitude and even sign of the surface excess elastic constants. The present study reports the variation in the effective macroscopic stiffness of bulk samples of nanoporous gold when the surface state is modulated under potential control in an electrochemical environment. Using *in situ* experiments in a dynamic mechanical analyzer to measure the storage and loss moduli, we show that adsorption of $\leq 1$ atomic monolayer of oxygen species as well as a capacitively controlled excess of electrons at the surface stiffen the material while oxygen desorption/electron depletion enhance the compliance. Relative changes in the effective stiffness of up to 8% imply the variation of a surface excess elastic constant in the order of 60 N/m, much larger than the absolute value of that constant deduced from previous atomistic simulation studies of clean surfaces. Since the electrode potential affects exclusively the surface, our observations provide conclusive evidence for the impact of local stiffness variation at surfaces on the effective elastic response of nanostructures.

*Keywords:* Surface excess elasticity, Surface stress, Nanoporous, Dynamic mechanical analysis, Nanostructures

## 1. Introduction

Solid surfaces interact with the underlying bulk via a capillary force, the surface stress, which takes on a finite value in the strain-free state of the surface [1]. The surface-stress variation with strain defines surface excess elastic moduli [2] which, for nanoscale objects or nanomaterials, entail a size-dependent effective elastic response of the entire structure. This is of interest whenever nanoscale objects undergo controlled elastic deformation, as in interpenetrating phase nanocomposites [3] or high-frequency microelectromechanical resonators [4], or when capillary forces define the materials function, as in cantilever-based sensors [5] or nanoporous metal actuators [6]. In spite of the considerable impact of surface excess elasticity, there is as yet no confirmed experimental picture of magnitude or even sign – stiffening or softening – of the effect. Here, we report experiments on the effective elastic response of nanoporous gold, a material with an extremely large specific surface area. Rather than seeking absolute values of the surface excess elastic modulus, our study focuses on reversible changes of the material's effective elastic response when the state of the surfaces is reversibly tuned. As we find large changes in the materials behavior, our experiments conclusively demonstrate the impact of surface excess elasticity on the elastic response of nanomaterials. We also point out that our approach yields a material with electrically tunable stiffness and with, thereby, a novel type of functionality.

Continuum theory relates the elastic response of the surface to the various deformation measures, such as the projection of the bulk strain onto the local tangent plane at the surface [2, 7]. Atomistic computation using embedded atom method (EAM) potentials generally indicates an enhanced compliance of transition metal surfaces [8, 9], while density functional theory (DFT) also allows for local stiffening, depending on the electronic structure of the surface [10]. Studies in continuum mechanics, as reviewed in [11], have adopted the EAM results in predicting the size-dependent effective elastic response for nanoscale objects. Yet, the applicability of EAM potentials for the problem has not been confirmed, and experimental verification is required. So far, the results of experiments with nanobeams and nanowires remain contradictory. With decreasing size, both stiffening (Pb, Ag, Pd, ZnO) [12–15] and softening (Si, Cr) [16, 17] have been reported in different materials. There are also experiments showing no size-dependence [15]. However, the implications for the surface elasticity may often be questioned, since either the materials investigated were relatively large ($\geq 50$ nm in size) [18–20] and hence poorly suited to probe surface behavior, or the accuracies of modulus and/or geometry measurements were low [21]. Furthermore, it has been

*Corresponding author. Tel: +49 4152 87-2617.
*Email address:* nadiia.mameka@hzg.de (Nadiia Mameka)

demonstrated that higher order elasticity in the bulk of nanowires may strongly affect their elastic response and control the size-dependence [9, 14]. From an experimental point of view, one may therefore question if the surface excess elasticity has any confirmed impact on the elastic response of nanomaterials at all.

Our study uses nanoporous gold (np-Au) made by alloy corrosion. The material takes the form of macroscopic (mm- or cm-size) bodies of metal distinguished by a low solid fraction ($< 1/2$) and by interpenetrating solid and pore phases with characteristic length scales that can be tuned between 5 nm and microns [22–24]. As predicted by the Gibson-Ashby foam scaling equations [25], the porosity drastically reduces the stiffness relative to massive gold. Most experiments on np-Au find effective stiffness values considerably below the Gibson-Ashby prediction for the respective solid fraction [26, 27], even though an enhanced stiffness has also been reported [28]. Recent modeling highlights the role of microstructural disorder in enhancing the effective compliance [29]. At present, the state of the art does not afford a sufficiently accurate modeling of the elastic response of porous solids for discussing the deviations between experiment and model in terms of contributions of the surface elasticity.

Nanoporous gold can be made to undergo self-similar structural coarsening while solid fraction and structural topology remain invariant [22]. This provides a meaningful way of analyzing the size-dependent elastic response. Relevant experimental data, as compiled in Refs. [24, 26, 28], typically find little or no systematic dependence on structure size, yet two studies report a rise of the stiffness when the ligament diameter drops to $< 10$ nm [28, 30]. This latter observation would indicate a positive excess elastic constant, in contrast to the often cited simulation results [8]. In view of the considerable uncertainties in such studies, our approach works with one and the same, stationary microstructure and explores the reversible variation of the elastic response as the surface state is cyclically varied. This has parallels to studies of the surface stress, where experiments on absolute values are scarce but where the variation during adsorption from gas and during electrosorption or capacitive charging in electrolyte has been accurately measured [31–33]. Specifically, we exploit the precise control of the surface states through electric potentials that can be achieved at the metal-electrolyte interface.

## 2. Phenomenological description of excess elasticity

As a background for discussing the mechanics of the solid/electrolyte interface we briefly expose the phenomenological approach, basing the notation on Ref. [34]. The impact of the surface on the energetics of elastic deformation is described by the surface free energy function $\psi(q, e)$ with the state variables $e$, the relative change in area by elastic strain, and $q$, the superficial charge density. The energy-conjugate variables to $e$ and $q$ are the scalar surface stress, $f$, and the electrode potential, $E$, so that $\mathrm{d}\psi = E\mathrm{d}q + f\mathrm{d}e$. The restriction to the scalar variables $e$ and $f$ is appropriate for surfaces with at least threefold rotational symmetry [1], such as the dense-packed surfaces of face-centered cubic metals in the limit of small strain. The associated surface excess elastic constant is then

$$\mathbb{C} = \frac{\partial^2\psi}{\partial e^2} = \frac{\mathrm{d}f}{\mathrm{d}e}|_q \,. \tag{1}$$

Even isotropic surfaces require an additional excess elastic constant that describes the development of surface stress anisotropy in response to in-plane shear. Yet, the documented experimental signatures of surface stress relate practically exclusively to the scalar parameter $f$, while information on surface stress anisotropy has been resolved only in few exceptional cases (such as Ref. [35] for Si). This prompts us to ignore excess shear stiffness and focus on area strain and the associated parameters $f$ and $\mathbb{C}$ alone.

Two other derivatives of $\psi$ are of relevance to the mechanics of electrodes. The electrocapillary coupling coefficient $\varsigma$ [34] describes how $f$ varies when the surface is charged, $\varsigma = \partial^2\psi/\partial e\partial q = (\mathrm{d}f/\mathrm{d}q)|_e$, and one may, in an analogous way, introduce an electro-elastic coupling parameter, $\lambda$, to describe elastic modulus variation with the surface charge:

$$\lambda = \frac{\partial^3\psi}{\partial e^2\partial q} = \frac{\mathrm{d}\mathbb{C}}{\mathrm{d}q}|_e \,. \tag{2}$$

It has been pointed out that the impact of capillarity on the effective stiffness of nanostructures may be parameterized by a simple geometric measure that rescales the dimensions of the nanoscale object [36]. In an attempt at illustrating the magnitude of $\mathbb{C}$, we adopt that concept to our notation. To this end, we consider the straining of an elastically isotropic slab, representing a square patch of thin film of edge length $l$ and thickness $t$, by in-plane forces $F_1$ and $F_2$ attached to two opposite cross-sectional faces (Fig. 1). In the absence of capillary effects, simple

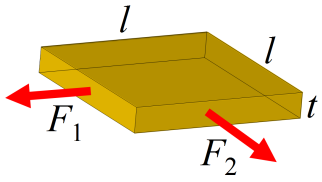


Figure 1: Schema of a cuboid slab, representing a patch of thin film of area $l \times l$ and thickness $t$, loaded on two opposite cross-sectional faces by the forces $F_1$ and $F_2$.

linear elasticity of isotropic media relates the area strain $e$ to the sum of the forces, $F = F_1 + F_2$ via $F = ltBe$, where $B$ denotes the biaxial modulus of the bulk of the film, $B = Y/(1-\nu)$ with $Y$, Young's modulus and $\nu$, Poisson's ratio of the bulk. Adding surface excess elasticity,

and measuring $e$ relative to a reference state of the film at $F = 0$, we have

$$F = ltBe + 2l\mathbb{C}e\,, \tag{3}$$

where the extra term accounts for the change in the surface stress that acts along the edges bounding the upper and lower (hence the factor 2) surfaces. Eq. (3) may equivalently be written as

$$F = l(t + 2\tau)Be\,, \tag{4}$$

where $\tau$ is defined as

$$\tau = \mathbb{C}/B\,. \tag{5}$$

By its definition through Eq. (5), $\tau$ is simply a parametrization of the surface excess elastic constant $\mathbb{C}$. Eq. (4) implies an intuitive geometric meaning of $\tau$. That parameter represents an effective thickening (for $\mathbb{C} > 0$) or thinning ($\mathbb{C} < 0$) of the effective film cross section in order to match the actual elastic response of the film of thickness $t$ (and with capillarity) by that of a thicker or thinner equivalent film that has no capillarity. The argument applies to more general geometries, and it implies that by working with $\tau$ instead of $\mathbb{C}$ one replaces the excess elastic constant of the surface with an apparent excess thickness (or an apparent specific excess volume) as the materials parameter. Even though the above exercise appears trivial, we shall use it profitably in the discussion of our experimental results.

We emphasize that the apparent excess thickness $\tau$ is merely a formal parametrization of the excess stiffness; $\tau$ has no relation to the actual inward or outward relaxation at the surface or to the physical specific excess volume, which are defined separately (see Refs. [34, 37]).

The estimates in Ref. [36], based on EAM-potentials, put the value of $\tau$ for the example of Al and Si surfaces in the order of $-100$ pm. For gold, with isotropic (polycrystalline) elastic constants $Y = 78$ GPa and $\nu = 0.44$, Eq. (5) would associate that $\tau$-value with $\mathbb{C} = -14$ N/m.

## 3. Experimental procedure

The synthesis of np-Au used procedures identical to Ref. [38] except were explicitly stated. In brief, ingots of the master alloy of $Au_{25}Ag_{75}$ were produced by arc melting, homogenized in a high-temperature anneal, shaped by wire drawing and cutting with a wire saw, annealed for recovery and then electrochemically dealloyed at ambient temperature using the potential 0.75 V in 1 M $HClO_4$. All potentials in this work are measured and quoted relative to the Ag/AgCl (pseudo) reference electrode in the same electrolyte, for which we measure +0.515 V *vs.* the standard hydrogen electrode (SHE).

In order to remove residual Ag, the dealloying was followed by polarization at potential 1.1 V in a fresh electrolyte until the current dropped below 10 $\mu A$. The as-dealloyed samples then underwent 20 potential cycles in the interval $-0.5$ to 1.0 V (scan rate 5 mV/s) to remove surface and subsurface oxides. The residual silver content, as determined by energy-dispersive x-ray spectroscopy in the scanning electron microscope (SEM) was then $< 1$ at.%. Subsequently, the samples were repeatedly rinsed with ultrapure water (18 M$\Omega$) and dried in Ar flow for several days. Samples were cylindrical, $1.17 - 1.20$ mm in diameter and $1.90 - 2.10$ mm in length.

Ligament size was determined by evaluating diameters in scanning electron micrographs. Taking into account the samples' mass and dimensions after dealloying and drying, the solid volume fraction of the as-prepared samples was $\phi = 0.26 \pm 0.01$.

Compression tests on dry samples were run at room temperature using a Zwick Z010 TN testing frame with a calibrated load cell, with the deformation monitored by a laser speckle extensometer (Zwick laserXtens) focusing on the load surfaces. The engineering strain rate was held constant at $10^{-4}$ s$^{-1}$. Unload/load segments from different prestrains, at the same strain rate, served for determining the effective (macroscopic) Young's modulus, $Y^{\text{eff}}$.

Dynamic mechanical analysis (DMA) in compression mode was carried out for quantifying changes in $Y^{\text{eff}}$ in response to potential change. Using a DMA 242C (Netzsch), we applied cyclic loading at frequency 1 Hz under strain control with peak-to-peak amplitude $\hat{\varepsilon} = 0.76\%$, superimposed to a static load of 2.1 N (corresponding to a static effective macroscopic stress of 1.9 MPa). A glass cuvette (Hellma) served as the *in situ* electrochemical cell while the load was applied via a quartz pushrod. All *in situ* experiments were conducted in 1 M $HClO_4$ (Suprapur, Merck). A larger sample of np-Au formed the counter electrode. The potential was controlled via a potentiostat (PGSTAT 302N, Metrohm). The electrode charge was obtained by integrating the current.

## 4. Results

### *4.1. Compression tests*

Np-Au with a ligament size of $L = 40 \pm 5$ nm was used throughout the present study (inset of Fig. 2a). We first inspect the elastic properties of dry samples in compression. The true stress–true strain curve of Fig. 2a is characterized by immediate plasticity even at the lowest strain, with no distinguishable yield point. This agrees with previous results for compression of macroscopic np-Au samples of similar ligament diameter [3, 39]. The analysis of the unload/load segments confirms the pronounced increase in the stiffness as the plastic deformation proceeds (Fig. 2b) that has been pointed out in Ref. [29].

### *4.2. Dynamic mechanical analysis*

Owing to their large compliance, which is similar to that of polymers, the porous metal samples are well compatible with the load range of a DMA. Prior to DMA experiments, samples were predeformed to a true strain in

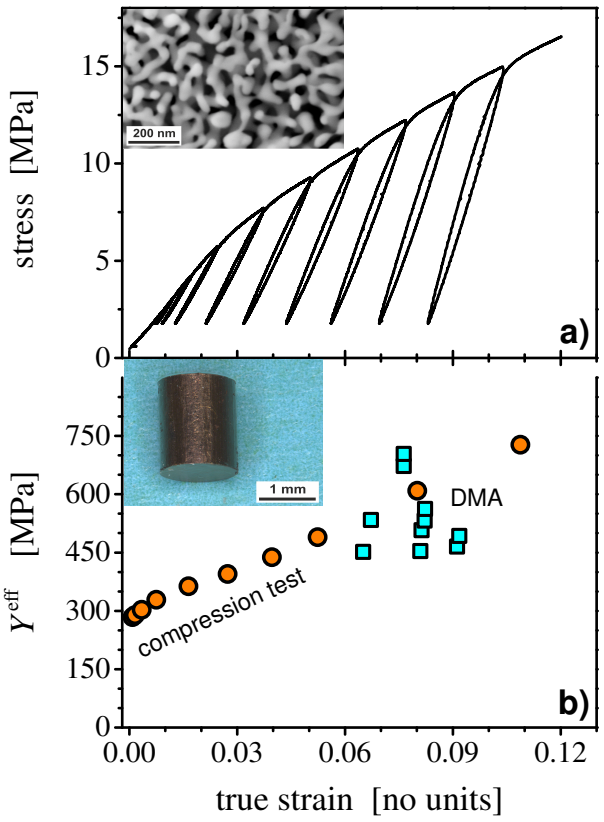


Figure 2: Compression behavior of np-Au: a) load-unload stress-strain diagram for engineering strain rate $9.5 \times 10^{-5}\ s^{-1}$. Inset: scanning electron micrograph of nanoporous microstructure. b) Variation of effective Young's modulus, $Y^{\rm eff}$, as determined from the load/unload segments, with strain (circles). Also shown (squares) is $Y^{\rm eff}$ as measured independently in the dynamic mechanical analyzer, using prestrained samples. Both data sets are seen to be consistent. Inset: photograph of typical sample.

the range of $0.065 - 0.09$ to provide coplanar loading surfaces. The effective macroscopic stiffness values obtained by DMA on several samples are shown in Fig. 2b for comparison with the results from the unload/load cycles during the conventional compression test. It is apparent that the two data sets for $Y^{\rm eff}$ are consistent. This supports the validity of the DMA data. Below we shall focus on studies probing the *relative changes* in the elastic response. These relative changes can be sensitively detected, irrespective of the degree of uncertainty in the absolute values.

The DMA experiment worked with the pore space of the np-Au wetted by 1 M $HClO_4$ as a weakly adsorbing aqueous electrolyte. The metal network was wired as the working electrode and the polarization of the metal-electrolyte interface controlled by a potentiostat. This *in situ* environmental control allowed us to probe changes in the elastic behavior of np-Au in response to varying the state of the surface. The approach was similar to that for electrochemical actuation studies by dilatometry [40]. Note the distinct difference between the electric and mechanical cycles. As each cyclic voltammogram took 1400 s, the corresponding frequency was $< 1$ mHz, more than three orders of magnitude slower than the mechanical cycles at 1 Hz. Therefore, each mechanical cycle was approximately at constant potential, and the mechanical and electric changes could be reliably separated.

Fig. 3 summarizes results of the *in situ* experiment, starting out in part a) with a cyclic voltammogram (CV) of electrode current versus electrode potential during a cyclic potential scan at 2 mV/s. The CV exhibits the well-known features of gold in acidic solutions, with oxygen species electrosorption peaks at the positive end and an extended capacitive regime at lesser potentials. Electrochemical studies of gold surfaces have established that the electrosorption under the present conditions is initiated by the deposition of 1 atomic monolayer of OH (peak at $\approx +0.8$ V), followed by gradual desorption of the hydrogen at more positive $E$ [41]. The adsorbate layer is reversibly desorbed during the negative-going scan. At +0.425 V, the open circuit potential of as-prepared samples was that of a clean surface, confirming that the reduction treatment during synthesis removed all superficial oxide. We also note that the potential of zero charge (pzc) of Au in 1 M $HClO_4$ is +50 mV on our potential scale (or 565 mV *vs.* SHE [42]), so that the scan in the capacitive regime covers regions of both, positive and negative surface charge.

Fig. 3b reports various aspects of the mechanical characterization, which was measured simultaneously with the cyclic voltammograms. The length change, $\Delta l$, represents a variation of the mean sample length, averaged over each of the fast load cycles. It is seen that $\Delta l$ undergoes a cyclic variation, with the length a monotonous function of the potential. This behavior, as well as the peak-to-peak amplitude of $0.063\% \pm 0.004\%$, is consistent with previous reports on the potential-induced strain of np-Au [40, 43]. The cyclic strain responds to a variation in the surface stress when the electrode is charged, and the expansion with increasing potential is consistent with a negative value of the electrocapillary coupling parameter $\varsigma$ for Au surfaces in the potential regime of our experiment [33]. In view of the reported impact of higher order bulk elasticity on the elastic response of nanowires at strains of several % [14] it is significant that the surface-induced strain amplitude is quite small here, so that its consequences for the bulk elastic constants may be ignored in our experiments.

The key observation in Fig. 3b is that the effective storage and loss moduli, which we denote by $Y'$ and $Y''$ for brevity, exhibit a large cyclic variation. Most remarkable is a strong increase of $Y'$ during oxygen electrosorption around the positive potential vertex. At the same time, $Y''$ decreases to less than half its clean-surface value. A second maximum in $Y'$ is observed at the negative potential vertex, while no significant feature in $Y''$ is resolved in that region. The observations suggest that both positive electric charging during oxygen electrosorption and negative charging during capacitive processes enhance the

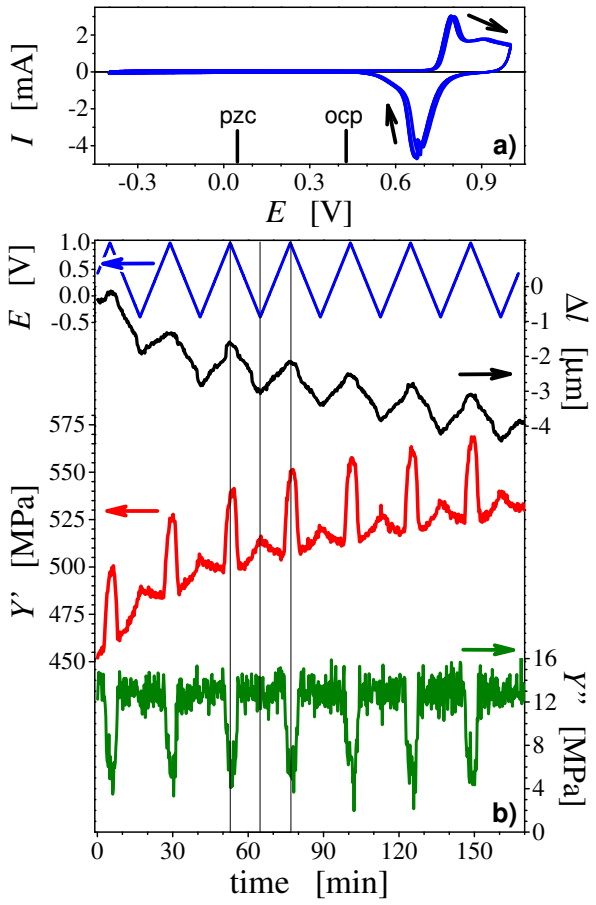


Figure 3: Results of dynamic mechanical analysis measured *in situ* during 7 successive cyclic scans of the electrode potential $E$ between $-0.4$ and $+1$ V, using 1 M $HClO_4$ as the electrolyte. a) Electrochemical characterization, represented by cyclic voltammograms (CVs) of current $I$ versus electrode potential $E$ at scan rate 2 mV/s, with scan direction indicated by arrows. Potential of zero charge (pzc) and open circuit potential (ocp) are also indicated. b) Mechanical characterization recorded simultaneously with the CVs, with variation of $E$ with time indicated by blue line and upper left ordinate: length change (black, upper right ordinate), storage modulus $Y'$ (red, lower left ordinate), and loss modulus $Y''$ (green, lower right ordinate). Vertical lines mark vertex points of CV for one exemplary cycle.

stiffness. Note that this behavior is qualitatively different from the monotonous potential-dependence of the length change. At any potential, the loss modulus remains small in comparison to the storage modulus, indicating a nearly ideal elastic behavior.

Superimposed to the cyclic changes is a slow upward drift of $Y'$. This stiffening coincides with an irreversible densification, with a shrinkage $\Delta l \sim -4$ $\mu$m or $-0.2\%$ of the initial length after the 7 cycles. Similar behavior is typically observed during potential cycles with nanoporous metals, and may arise from slow plastic deformation under the action of the surface stress [6]. Since the cyclic changes in length and elastic response remain invariant, the impact of the densification on the material's behavior of interest appears negligible.

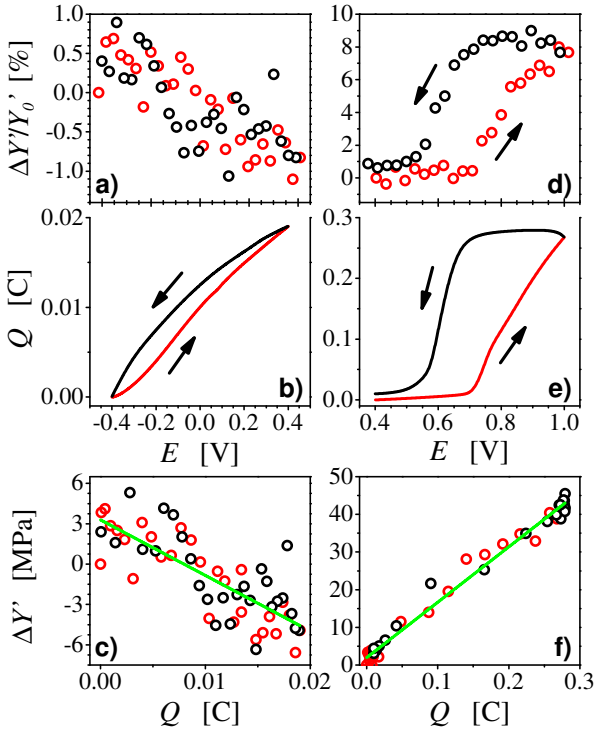


Figure 4: Relative variation of the storage modulus $\Delta Y'/Y_0'$ of np-Au electrode at two distinguishable surface states: a) $\Delta Y'/Y_0'$ vs. $E$ in capacitive double-layer regime and b) charge associated with charging and discharging processes of electrical double layer. d) $\Delta Y'/Y_0'$ vs. $E$ in adsorption-desorption region and e) corresponding charge transfer attributed to the oxidation and reduction reactions. c) and f) $\Delta Y'$ as a function of charge $Q$ for both states. $\Delta Y' = f(Q)$ exhibits a reasonably linear behavior with slopes $-413.62 \pm 43.41$ MPa/C and $147.08 \pm 2.99$ MPa/C. Electrolyte is 1 M $HClO_4$, scan rate is 2 mV/s. Arrows indicate the direction of scan.

Additional *in situ* DMA measurements explore two separate potential windows from the scans of Fig. 3, namely capacitive polarization ($E = -0.4...0.4$ V) and oxygen species electrosorption ($E = 0.4...1.0$ V). Fig. 4 summarizes the results. Part d) of Fig. 4 shows that OH adsorption leads to an increase in $Y'$, in direct proportion to the electrode charge, $Q$, as displayed in Fig. 4e. Backward (cathodic) scanning initially leaves $Y'$ constant with the adsorbate layer remaining in place. Further potential reduction leads to oxygen desorption, with the stiffness reverting to its initial, lower value. In fact, a linear and hysteresis-free relation is obtained when plotting $Y'$ versus $Q$ for both scan directions (Fig. 4f). We have repeated this experiment on a set of five separate samples from different batches and found highly consistent results, with the relative change in storage modulus of $7.8 \pm 0.9\%$.

The second potential window inspects the capacitive regime. The potential scans here reveal a linear variation of the storage modulus with potential (Fig. 4a) and charge (Fig. 4b and 4c). As compared to oxygen electrosorption, the slope during capacitive charging is of inverse sign, with

negative charge or surface excess of electrons stiffening the material. The overall variation in $Y'$, again determined independently with five samples, here attained $1.6 \pm 0.1\%$.

## 5. Discussion

In relation to the effective Young's modulus we note that our result for $Y^{\text{eff}}$ at the onset of deformation is at least one order of magnitude lower than what was deduced in several previous reports on nanoporous gold. Experiments using nanoindentation, film bending, and microtensile or compression tests found $Y^{\text{eff}}$ in the range $3 - 13$ GPa for ligament sizes of $20 - 40$ nm [30, 44, 45]. It is therefore significant that we obtained consistent results with a series of samples from different batches. These samples are of the crack-free type that our earlier studies have shown to be perfectly deformable in compression [38, 39] and to yield strong and ductile nanocomposites when infiltrated with polymer [3]. We therefore rule out structural imperfections such as native cracks as a possible origin of the large compliance. A possible explanation attributes the higher stiffness reported by other authors to densification during loading (in the case of nanoindentation) or synthesis (thin films). Compared to other methods, our conventional mechanical testing of mm-sized samples appears a conservative and reliable method, supporting our result.

As the most important aspect of the *in situ* DMA data we advertise the implications for the surface excess elasticity. As the electrochemical cycles affect the material exclusively at its surface, the changes in the effective elastic response are forcefully the signature of a variation in $\mathbb{C}$. Our results therefore conclusively establish that local changes in the stiffness at surfaces can significantly affect the macroscopic elastic response of nanomaterials. The significance of this observation rests specifically on its nature as a reversible modulation of the elastic response of a given sample. While the effective stiffness varies, the geometry of the microstructure remains invariant. This rules out artifacts from incorrect or imprecise reference data, which can arise when surface contributions are to be derived from absolute values of the elastic response of a nanomaterial or nanoscale object. In such instances, precise data for geometric dimensions, for crystallographic orientation and for the set of elastic coefficients of the material are crucial and not in all instances available. This complication is avoided in our approach.

Our phenomenological description of surface excess elasticity has introduced the parameters $\varsigma$ and $\lambda$, which quantify, respectively, the charge-dependencies of the surface stress and of the surface excess elastic constant $\mathbb{C}$. The observations on potential-induced strain in Fig. 3b confirm the established finding that $\varsigma$ of clean Au surfaces is of same (negative) sign for capacitive charging and for oxygen species electrosorption [33, 40]. By contrast, the data for $Y^{\text{eff}}$ *vs.* $q$ in Fig. 4c and 4f imply that $\lambda$ takes on different signs, negative for capacitive surface charging and positive during oxygen species electrosorption.

Going beyond the observations on the sign and establishing a precise link between $\lambda$ and the variation in $Y^{\text{eff}}$ requires continuum theory for *i)* the elasticity of solid networks with realistic geometry and *ii)* the impact of surface excess elasticity on networks with a nanoscale structure size. Research on issue *i* is ongoing with increasingly detailed models [29, 46], yet predictions with the required precision of much better than the magnitude of our effect $(2 - 8\%)$ are as yet unavailable. Issue *ii* has seen computations restricted to model geometries [47, 48] that do not approximate the microstructure of np-Au, and even the simpler problem of predicting the response of the strain to the surface stress is afflicted with uncertainties of several 10% [43].

In view of the above concerns, we propose an order-of-magnitude estimate of the change in $\mathbb{C}$. The elastic deformation of not too dense network solids, such as nanoporous gold, is dominated by the bending deformation of the struts or ligaments [29]. In other words, Bernoulli beam theory [49] applies, and the relevant geometry parameter for the bending stiffness is the second moment of inertia of the ligaments, $I = {}^1\!/_4 \pi r^4$ with $r$ a characteristic ligament radius. In the spirit of Eqs. (4) and (5), the change in excess elasticity may be represented by an apparent small variation in ligament radius, which may then be identified with a change in the apparent surface specific excess volume $\tau$. We thus take $\delta I = (\mathrm{d}I/\mathrm{d}r)\delta\tau$, which implies that the relative change in bending stiffness agrees with

$$\frac{\delta I}{I} = \frac{4}{r}\delta\tau\,. \tag{6}$$

Assuming linear elasticity, the relative change in stiffness of the ligament as the single constitutive structural element agrees with the relative change of the macroscopic stiffness. Therefore, the relative changes in $Y^{\text{eff}}$ by 7.8 and 1.6% in the two potential regions investigated correspond to numerically identical relative changes in $I$. With $r \approx 22$ nm (half the ligament diameter), and using Eq. (6), we obtain for $\delta\tau$ the values 430 and 88 pm. This compares to estimates for the absolute value of $\tau$ in the order of 100 pm [36]. Eq. (5) then implies changes in $\mathbb{C}$ in our experiments by 60 N/m (electrosorption) and 12 N/m (capacitive charging). For comparison, the uniaxial in-plane excess surface stiffness of the embedded-atom-potential approximation of Au(111) is $-8.0$ N/m [8]. Hence, the observed changes in $\mathbb{C}$ of our study are similar or even much larger than reported estimates of the absolute values of the surface excess stiffness at clean surfaces. This underlines the significance of the surface adsorbate coverage or electric polarization for the surface excess elasticity.

In relation to the variation in $\tau$ we also note that the lattice parameter of Au is $\sim 408$ pm and the spacing between dense-packed layers is $d_{111} = 235$ pm. In other words, in order to account for the effective stiffening of np-Au samples during adsorption of 1 atomic monolayer

of OH by the hypothetical process of simply adding extra Au on the surface, one would need to add a layer with the thickness of more than a full lattice parameter or nearly two dense-packed layers of Au. These are huge effects, for instance in comparison to the actual change in excess volume during capacitive charging of Au in electrolyte, which is in the order of only 1 pm [50, 51].

In a quite general sense, the variation of the surface excess elasticity may be understood as the consequence of reversible changes of the bonding strength between the atoms at the surface. In the case of capacitive charging, the observed sign of $\lambda$ is consistent with a simple-minded picture in which excess electrons at a negatively charged surface will partly leak into the bonding regions of electron density in-between the surface layer of atoms [52]. This would be expected to enhance both the surface stress and the surface excess stiffness; in both instances the expectation agrees with our observation. Yet, the argument fails to explain the stiffening in the case of oxygen species electrosorption, where charge is expected to be transferred from the metal to the oxygen, leaving the surface depleted in electrons. The bond forces between the adsorbed OH and the Au might contribute to the surface stiffness, yet there are good arguments for ignoring such forces and attributing the impact of anion adsorption on noble metal electrode surfaces exclusively to the changes in the bonding between the metal atoms [32, 53, 54]. In our view, the state of the art on the capillarity of solids does not to afford a simple explanation for the considerable stiffening of the Au surface during oxygen species electrosorption.

The almost complete suppression of the loss modulus when oxygen species adsorb is remarkable. This would be consistent with a scenario where surface defects (step edges, kinks) rearrange in response to a variation of the heterogeneous strain fields on the surface. Upon oxygen adsorption, the rearrangement might be quenched along with the surface mobility of gold. Alternatively, the dissipative loss for the nominally clean surface might arise from the rearrangement of adatoms in varying strain fields at the surface, consistent with the reported trend for a decoration of strain fields by adatoms [55]. Weakly adsorbed anions such as sulfate are present at these potentials [56], and sulfate might indeed be an impurity in the electrolyte. Oxygen species are known to displace the anions from the surface [56]; since the oxygen is more strongly bound it may not rearrange in varying stress fields at the surface, thereby explaining the reduced loss.

## 6. Conclusions

In conclusion, our experiments demonstrate that the effective elastic modulus of np-Au in contact with an electrolyte can be controlled by the electrode potential. Adsorption of oxygen species as well as a simple excess of electrons in the surface are both found to reversibly increase the macroscopic stiffness. The relative changes in macroscopic stiffness for the two processes reach $\sim 8\%$ and $\sim 2\%$, respectively. In relation to the excess elastic response of the surface, these findings imply changes which are considerably larger than the absolute values that have been suggested by atomistic simulation using embedded atom potentials. Our findings conclusively establish the important impact of surface excess elasticity on the mechanical behavior of nanomaterials. They also show that this behavior is crucially dependent on the state of the surface, clean or adsorbate covered. The strong impact of small quantities of adsorbate may explain some of the discrepancies in earlier attempts to explore surface excess elasticity, in which the adsorbate coverage was not characterized.

As a direct consequence of the importance of surface elasticity, our findings also reveal a novel functionality of nanoporous metals, namely their electrochemically tunable stiffness. This supports the notion of modification of properties of nanometer-sized structures by means of electric signals [38, 57, 58].

## Acknowledgments

This work was supported by Deutsche Forschungsgemeinschaft through grant WE1424/14-1.

## References

[1] Shuttleworth R. The surface tension of solids. Proceedings of the Physical Society of London Section A 1950;63(365):444–57.
[2] Gurtin ME, Murdoch AI. Continuum theory of elastic-material surfaces. Archive for Rational Mechanics and Analysis 1975;57(4):291–323.
[3] Wang K, Weissmüller J. Composites of nanoporous gold and polymer. Advanced Materials 2013;25(9):1280–4.
[4] Husain A, Hone J, Postma HWC, Huang XMH, Drake T, Barbic M, et al. Nanowire-based very-high-frequency electromechanical resonator. Applied Physics Letters 2003;83(6):1240–2.
[5] Boisen A, Thundat T. Design & fabrication of cantilever array biosensors. Materials Today 2009;12(9):32–8.
[6] Jin HJ, Wang XL, Parida S, Wang K, Seo M, Weissmüller J. Nanoporous au-pt alloys as large strain electrochemical actuators. Nano Letters 2010;10(1):187–94.
[7] Gurtin ME, Weissmüller J, Larché F. A general theory of curved deformable interfaces in solids at equilibrium. Philosophical Magazine a-Physics of Condensed Matter Structure Defects and Mechanical Properties 1998;78(5):1093–109.
[8] Shenoy VB. Atomistic calculations of elastic properties of metallic fcc crystal surfaces. Physical Review B 2005;71(9):11.
[9] Liang H, Upmanyu M, Huang H. Size-dependent elasticity of nanowires: Nonlinear effects. Physical Review B 2005;71(24):241403.
[10] Zhou LG, Huang H. Are surfaces elastically softer or stiffer? Applied Physics Letters 2004;84(11):1940–2.
[11] Duan HL, Wang J, Karihaloo BL. Theory of elasticity at the nanoscale. Advances in Applied Mechanics, Vol 42 2008;42:1–68.
[12] Cuenot S, Fretigny C, Demoustier-Champagne S, Nysten B. Surface tension effect on the mechanical properties of nanomaterials measured by atomic force microscopy. Physical Review B 2004;69(16):165410.
[13] Jing GY, Duan HL, Sun XM, Zhang ZS, Xu J, Li YD, et al. Surface effects on elastic properties of silver nanowires: Contact atomic-force microscopy. Physical Review B 2006;73(23):235409.

[14] Chen LY, Richter G, Sullivan JP, Gianola DS. Lattice anharmonicity in defect-free pd nanowhiskers. Physical Review Letters 2012;109(12):125503.
[15] Qiao L, Zheng X. Effect of surface stress on the stiffness of micro/nanocantilevers: Nanowire elastic modulus measured by nano-scale tensile and vibrational techniques. Journal of Applied Physics 2013;113(1):013508.
[16] Li X, Ono T, Wang Y, Esashi M. Ultrathin single-crystalline-silicon cantilever resonators: Fabrication technology and significant specimen size effect on youngs modulus. Applied Physics Letters 2003;83(15):3081–3.
[17] Nilsson SG, Borrisé X, Montelius L. Size effect on youngs modulus of thin chromium cantilevers. Applied Physics Letters 2004;85(16):3555–7.
[18] Tabib-Azar M, Nassirou M, Wang R, Sharma S, Kamins TI, Islam MS, et al. Mechanical properties of self-welded silicon nanobridges. Applied Physics Letters 2005;87(11):113102.
[19] Ni H, Li XD. Young's modulus of zno nanobelts measured using atomic force microscopy and nanoindentation techniques. Nanotechnology 2006;17(14):3591–7.
[20] Chen YX, Dorgan BL, McIlroy DN, Aston DE. On the importance of boundary conditions on nanomechanical bending behavior and elastic modulus determination of silver nanowires. Journal of Applied Physics 2006;100(10):7.
[21] Müller P. Fundamentals of Stress and Strain at the Nanoscale Level: Toward Nanoelasticity. Wiley VCH; 2011, p. 27–59.
[22] Li R, Sieradzki K. Ductile-brittle transition in random porous au. Physical Review Letters 1992;68(8):1168–71.
[23] Erlebacher J, Aziz MJ, Karma A, Dimitrov N, Sieradzki K. Evolution of nanoporosity in dealloying. Nature 2001;410(6827):450–3.
[24] Weissmüller J, Newman RC, Jin HJ, Hodge AM, Kysar JW. Nanoporous Metals by Alloy Corrosion: Formation and Mechanical Properties; vol. 34. Warrendale, PA, ETATS-UNIS: Materials Research Society; 2009.
[25] Gibson LJ, Ashby MF. Cellular solids: structure and properties. Cambridge solid state science series; 2 ed.; Cambridge University Press; 1997.
[26] Biener J, Hamza AV, Hodge AM. Deformation Behavior of Nanoporous Metals; chap. 6. Springer US; 2008, p. 118–35.
[27] Hodge A, Doucette R, Biener M, Biener J, Cervantes O, Hamza A. Ag effects on the elastic modulus values of nanoporous au foams. Journal of Materials Research 2009;24(04):1600–6.
[28] Liu R, Antoniou A. A relationship between the geometrical structure of a nanoporous metal foam and its modulus. Acta Materialia 2013;61(7):2390–402.
[29] Huber N, Viswanath RN, Mameka N, Markmann J, Weißmüller J. Scaling laws of nanoporous metals under uniaxial compression. Acta Materialia 2014;67(0):252–65.
[30] Mathur A, Erlebacher J. Size dependence of effective young's modulus of nanoporous gold. Applied Physics Letters 2007;90(6):061910.
[31] Ibach H. The role of surface stress in reconstruction, epitaxial growth and stabilization of mesoscopic structures. Surface Science Reports 1997;29(56):195–263.
[32] Haiss W. Surface stress of clean and adsorbate-covered solids. Reports on Progress in Physics 2001;64(5):591–648.
[33] Weissmüller J. Electrocapillarity of Solids and its Impact on Heterogeneous Catalysis. Advances in Electrochemical Science and Engineering; Weinheim, Germany: Wiley VCH; 2013, p. 163–219.
[34] Weissmüller J, Kramer D. Balance of force at curved solid metal-liquid electrolyte interfaces. Langmuir 2005;21(10):4592–603.
[35] Métois JJ, Saúl A, Müller P. Measuring the surface stress polar dependence. Nature Materials 2005;4(3):238–42.
[36] Miller RE, Shenoy VB. Size-dependent elastic properties of nanosized structural elements. Nanotechnology 2000;11(3):139–47.
[37] Nozières P, Wolf DE. Interfacial properties of elastically strained materials .1. thermodynamics of a planar interface. Zeitschrift Fur Physik B-Condensed Matter 1988;70(3):399–407.
[38] Jin HJ, Weissmüller J. A material with electrically tunable strength and flow stress. Science 2011;332(6034):1179–82.
[39] Jin HJ, Kurmanaeva L, Schmauch J, Rösner H, Ivanisenko Y, Weissmüller J. Deforming nanoporous metal: Role of lattice coherency. Acta Mater 2009;57(9):2665–72.
[40] Jin HJ, Parida S, Kramer D, Weissmüller J. Sign-inverted surface stress-charge response in nanoporous gold. Surface Science 2008;602(23):3588–94.
[41] Conway BE. Electrochemical oxide film formation at noble-metals as a surface-chemical process. Progress in Surface Science 1995;49(4):331–452.
[42] Kolb DM, Schneider J. Surface reconstruction in electrochemistry - au(100)-(5x20), au(111)-(1x23) and au(110)-(1x2). Electrochimica Acta 1986;31(8):929–36.
[43] Shao LH, Jin HJ, Viswanath RN, Weissmüller J. Different measures for the capillarity-driven deformation of a nanoporous metal. Europhysics Letters 2010;89(6):66001.
[44] Lee D, Wei X, Chen X, Zhao M, Hone J, Herbert EG, et al. Microfabrication and mechanical properties of nanoporous gold at the nanoscale. Scripta Materialia 2007;56(5):437 –40.
[45] Balk TJ, Eberl C, Sun Y, Hemker KJ, Gianola DS. Tensile and compressive microspecimen testing of bulk nanoporous gold. JOM 2009;61(12):26–31.
[46] Sun XY, Xu GK, Li X, Feng XQ, Gao H. Mechanical properties and scaling laws of nanoporous gold. Journal of Applied Physics 2013;113(2):023505.
[47] Lu ZX, Zhang CG, Liu Q, Yang ZY. Surface effects on the mechanical properties of nanoporous materials. Journal of Physics D-Applied Physics 2011;44(39):395404.
[48] Xia R, Li X, Qin Q, Liu J, Feng XQ. Surface effects on the mechanical properties of nanoporous materials. Nanotechnology 2011;22(26):265714.
[49] Timoshenko SP, Goodier JN. Theory of Elasticity. 2 ed.; McGraw-Hill, New York; 1951.
[50] Nichols RJ, Nouar T, Lucas CA, Haiss W, Hofer WA. Surface relaxation and surface stress of au(111). Surface Science 2002;513(2):263–71.
[51] Umeno Y, Elsaesser C, Meyer B, Gumbsch P, Weissmüller J. Reversible relaxation at charged metal surfaces: An ab initio study. Europhysics Letters 2008;84(1):13002.
[52] Albina JM, Elsasser C, Weissmüller J, Gumbsch P, Umeno Y. Ab initio investigation of surface stress response to charging of transition and noble metals. Physical Review B 2012;85(12):125118.
[53] Haiss W, Nichols RJ, Sass JK, Charle KP. Linear correlation between surface stress and surface charge in anion adsorption on au(111). Journal of Electroanalytical Chemistry 1998;452(2):199–202.
[54] Smetanin M, Viswanath RN, Kramer D, Beckmann D, Koch T, Kibler LA, et al. Surface stress-charge response of a (111)-textured gold electrode under conditions of weak ion adsorption. Langmuir 2008;24(16):8561–7.
[55] Gsell M, Jakob P, Menzel D. Effect of substrate strain on adsorption. Science 1998;280(5364):717–20.
[56] Shi Z, Lipkowski J, Gamboa M, Zelenay P, Wieckowski A. Investigations of so4(2-) adsorption at the au(111) electrode by chronocoulometry and radiochemistry. Journal of Electroanalytical Chemistry 1994;366(1-2):317–26.
[57] Gleiter H, Weissmüller J, Wollersheim O, Würschum R. Nanocrystalline materials: a way to solids with tunable electronic structures and properties? Acta Materialia 2001;49(4):737–45.
[58] Weissmüller J, Viswanath RN, Kramer D, Zimmer P, Würschum R, Gleiter H. Charge-induced reversible strain in a metal. Science 2003;300(5617):312–5.